Earth and Planetary Science Letters 462 (2017) 86–98

Contents lists available at ScienceDirect

Earth and Planetary Science Letters

www.elsevier.com/locate/epsl

Symmetry during the syn- and post-rift evolution of extensional back-arc basins: The role of inherited orogenic structures

Attila Balázs [a,b,*], Evgueni Burov [c,1], Liviu Matenco [b], Katharina Vogt [b], Thomas Francois [b,c], Sierd Cloetingh [b]

[a] Department of Geophysics and Space Sciences, Eötvös Loránd University, Budapest, Hungary
[b] Netherlands Research Centre for Integrated Solid Earth Science, Utrecht University, Faculty of Geosciences, Utrecht, The Netherlands
[c] Université Pierre et Marie Curie, Institut des Sciences de la Terre de Paris, France

ARTICLE INFO

Article history:
Received 11 September 2016
Received in revised form 10 January 2017
Accepted 15 January 2017
Available online 30 January 2017
Editor: A. Yin

Keywords:
numerical modelling
extensional back-arc basins
weakness zone
Pannonian
Aegean

ABSTRACT

Rheological heterogeneities in the lithosphere have first order control on the topographical expression of tectonic processes. Pre-existing orogenic suture zones localise extensional deformation resulting in asymmetric basins. Such crustal geometries are often in contrast with the more symmetric regional lithospheric structure observed beneath extensional basins. We study such (a)symmetries and their controlling parameters by conducting a series of 2D thermo-mechanical numerical experiments of the extension of an overthickened, hot lithosphere that contains a weakness zone. The modelling shows that syn-rift subsidence is low to moderate creating asymmetric half grabens where extension migrates in space and time, grouped in an overall symmetrical appearance on a larger scale. The initial lithospheric mantle asymmetry is attenuated by the lateral heat conduction and further dynamic evolution of the thermal anomaly during the "post-rift" phase, resulting in differential vertical movements of the crust including additional 2–3 km subsidence in the basin centre. The modelling shows that the initial crustal and lithospheric thicknesses, rate of extension and surface processes strongly control the thermo-mechanical evolution of the extensional system. The numerical modelling yields new insights into the mechanics of coupling between near-surface kinematics and the evolution of deep lithospheric structure in the Pannonian basin and the Aegean, two of Europe's largest back-arc systems.

1. Introduction

The evolution of extensional basins is controlled by multiple internal and external forcing factors and parameters, such as variable plate divergent rates, surface processes, coupled or decoupled crustal and lithospheric configurations, evolution of asthenospheric thermal anomalies and associated mantle dynamics (e.g., Huismans and Beaumont, 2003; Burov, 2007; Liao and Gerya, 2014). Moreover, rheology is a key parameter influencing the geometry of extension, strength contrasts and degree of brittle–ductile coupling (e.g., Brun, 1999; Burov and Poliakov, 2001). It also controls localisation of deformation and its subsequent evolution (Dunbar and Sawyer, 1988; Sokoutis et al., 2007; Li et al., 2011). The extension rates also control the style of extension, for instance low divergence rates or tectonic quiescence periods may lead to rift migration (Van Wijk and Cloetingh, 2002; Naliboff and Buiter, 2015), critical for the formation of hyper-extended margins (Brune et al., 2014). Furthermore, low extension rates favour the formation of asymmetric basins, resulting in the creation of high lateral offsets between the locations of maximum crustal and lithospheric thinning (e.g., Huismans and Beaumont, 2003). Analogue models infer that different extension rates also have considerable impact on strain localisation. An increase of plate divergence rate increases the strength of the ductile layers and therefore enhances the coupling between the brittle and ductile layers resulting in more distributed extension (Brun, 1999; Corti et al., 2003).

The symmetry of extension, in terms of crustal and lithospheric thinning and its evolution with time, and the degree of rheological coupling between different lithospheric layers are particularly important when extension affects a pre-existing nappe stack (e.g., Ziegler and Cloetingh, 2004). In orogenic settings, nappe contacts provide critical rheological contrasts. In particular, subduction and suture zones formed during the amalgamation of continents provide the possibility of large lithospheric scale reactivations (e.g.,

* Corresponding author at: Department of Geophysics and Space Sciences, Eötvös Loránd University, Pázmány Péter st. 1/C, H-1117 Budapest, Hungary.
E-mail address: a.balazs@uu.nl (A. Balázs).

[1] Professor Evgueni Burov has passed away on 9th October 2015.

http://dx.doi.org/10.1016/j.epsl.2017.01.015
0012-821X/

Dunbar and Sawyer, 1988; Sokoutis et al., 2007). Such conditions are most often met in extensional back-arc domains, where asymmetric (i.e., simple shear) extension reactivates suture zones and nappe contacts shortly after orogenic build-up, affecting an overthickened, hot and weak lithosphere (Le Pourhiet et al., 2004; Tirel et al., 2008; Huet et al., 2011; Menant et al., 2016). Back-arc extension reactivates thrust contacts and exhumes rocks previously buried at great depths, such as in the Apennines or Aegean system (e.g., Brun and Faccenna, 2008). In these settings deformation occurs at high strain rates, controlled by the interplay between subduction and plate convergence velocities, such as typically observed in Mediterranean back-arcs. Extension was variable in time and space with average velocities of 2–3 cm/yr for the last 30 My, of course short periods of very slow and fast extensional pulses are inferred (Faccenna et al., 2014).

The role of evolving thermal anomalies, phase transformations and migration of deformation in space and time associated with variable subsidence rates are important in understanding the evolution of extensional basins, in particular in back-arc settings (Cloetingh et al., 2013; Menant et al., 2016). Numerical models have demonstrated the close feedback between stretching, evolution of thermal anomalies and basin formation (Huismans and Beaumont, 2003; Burov, 2007). However, their relationship with the extensional back-arc basin infill, in terms of symmetry, evolution and migration of deformation in time and space, is less understood.

In this study, we investigate the influence of large scale rheological weakness zones during the formation and evolution of back-arc extension using 2D thermo-mechanical numerical modelling calibrated by geological and geophysical observations. A key element in our model is the implementation of a lithospheric weakness zone, simulating the influence of a pre-existing suture or major nappe contact during extension. We conducted a series of numerical models to test the controls of key parameters, such as the initial crustal and lithospheric thicknesses, weakness zone geometry, extensional velocities applied at the model sides and rate of erosion and sedimentation. Our study focuses on analysing the influence of these parameters on the interplay between the extensional symmetric versus asymmetric crustal deformation and mantle structure, and the formation and evolution of the overlying sedimentary basins. Our numerical modelling results are compared to observations in two of Europe's largest extensional back-arc areas, the Pannonian and Aegean basins of the Mediterranean region.

2. Modelling methodology

Thermo-mechanical numerical modelling is particularly well suited to study the mechanics of extension and the evolution of associated sedimentary basins (e.g., Burov and Poliakov, 2001; Huismans and Beaumont, 2003). We have employed the thermo-mechanically coupled 2D finite element code Flamar v12 (e.g., Francois et al., 2013; Burov and Gerya, 2014), based on the earlier Flac-Para(o)voz algorithm (e.g., Poliakov et al., 1993). Because of its capability to solve for large strains and its free upper surface boundary condition, this method is especially suitable to monitor the surface vertical movements during basin (de)formation (Fig. 1). The numerical algorithm explicitly takes into account elasto-visco-plastic properties of different lithospheric layers and the asthenosphere. The implemented constitutive laws include linear elasticity, Mohr–Coulomb failure criterion for brittle deformation (faults) and pressure–temperature and strain-rate dependent viscous deformation (Ranalli, 1995). Linear cohesion softening is used for effective localisation of plastic deformation (e.g., Huismans and Beaumont, 2003). Our modelling setups involve a 2D section of 1000 km wide and 450 km deep. Constant lateral velocities are applied at the sides, while the upper boundary is a free surface (Burov and Poliakov, 2001). Pliable lithostatic pressure (Winkler basement) is applied at the bottom of the model, which implies vertical normal stresses proportional to vertical displacement of the boundary, multiplied by the density contrast (see also Burov, 2007; Francois et al., 2013). The horizontal grid resolution is 2 km and the vertical grid resolution varies between 1.2 up to 3 km, with higher resolution in the upper part of the crust and the overlying sedimentary basin (Fig. 1). The accuracy of vertical displacements is in the order of 10 meters based on a series of sensitivity analyses (see Appendix and Francois et al., 2013).

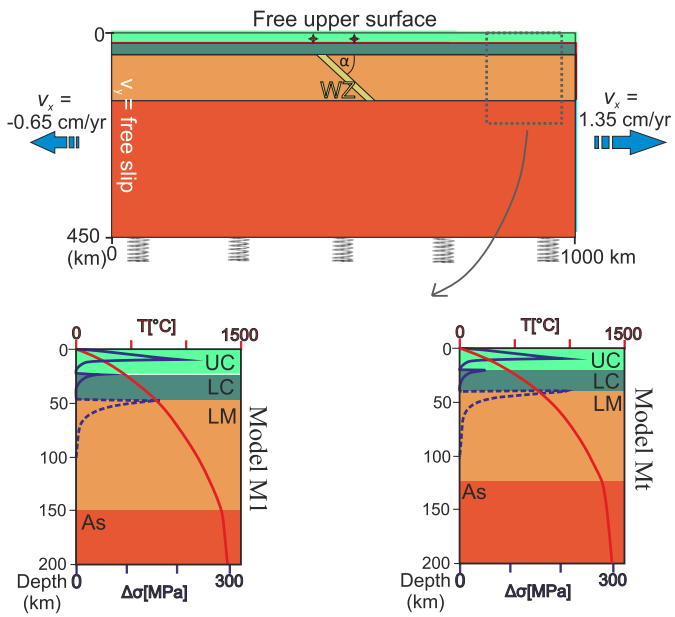

Fig. 1. Initial setup of the numerical model. The upper model boundary is a free surface. Springs indicate lithostatic pressure (Winkler basement) applied at the base of the model. Constant lateral velocities are applied at the sides of the model (blue arrows). An initial tilted rheological weak zone (WZ) is defined in the lithospheric mantle. Two crustal marker points are plotted on the phase configuration showing the evolution of extension with time in Fig. 2. The initial geotherms and strength profiles were calculated for model M1 (left) and Mt (right) based on the rheological parameters of Table 1. UC: upper crust, LC: lower crust, LM: lithospheric mantle, As: asthenosphere. The lithospheric mantle is relatively weak (dashed line) due to the high geotherm and has no strength at the weakness zone at such high temperature values. (For interpretation of the references to colour in this figure, the reader is referred to the web version of this article.)

The experiments are specifically designed to simulate the fast extension of a hot and overthickened lithosphere that is common to many back-arc areas preceding extension, for instance in the Alpine-Carpathian region (Fig. 1; Faccenna et al., 2014). Our modelling procedure includes the implementation of a reference model (model M1, Table 1) and further analysis of the effects of variable parameters, such as rate of erosion and sedimentation, lithospheric weakness zone dip angle, initial crustal and lithospheric thickness and the rate of extension. A setup with an initial crustal thickness of 48 km, lithospheric thickness of 150 km, lithospheric weakness zone dip angle of 50 degrees with lateral velocities of 0.65 cm/yr left and 1.35 cm/yr right has been defined as a reference model for comparison with other scenarios (Figs. 1 and 2, Table 1). Similar to other numerical models (Burov and Poliakov, 2001), surface processes in terms of erosion and sedimentation were simulated by a linear diffusion law, where different erosion coefficients (k_e) correspond to different erosion rates (Table 1). Such an approach allows us to consider the dependence of erosion and sedimentation rate on the smoothness of the relief (i.e. surface curvature). The influence of the surface processes is simulated by a variable erosion coefficient (k_e) between 0 to 750 $m^2\,yr^{-1}$.

Table 1
Basic parameters of the 17 presented model experiments. Rheological parameters are adapted from similar numerical experiments (upper crust: e.g., Burov, 2007; Cloetingh et al., 2013; lower crust: e.g., Francois et al., 2013; mantle: e.g., Burov and Poliakov, 2001; and Ranalli, 1995). Model Mo with much lower geotherm is presented in Appendix A.

Length of models x_L	1000 km
Amount of extension	190–260 km
Temperature at the base of the lithosphere	1300 °C
Radioactive heat production, H_s	1.5×10^{-9} W kg^{-1}
Radiogenic production decay length, h_r	10 km
Crustal thermal conductivity, k_c	2.5 W K^{-1} m^{-1}
Mantle thermal conductivity, k_m	3.3 W K^{-1} m^{-1}
Thermal diffusivity of mantle, χ	10^{-6} m^2 s^{-1}
Specific heat, C_p	1000 J K^{-1} kg^{-1}
Cohesion	20 MPa

	Upper crust	Lower crust	Mantle lithosphere	Weak zone	Asthenosphere
Thickness (km)	24, 20	24, 20	102, 95	–	300, 315
Density, ρ_0 (kg m^{-3})	2750	2900	3330	3270	3330
Power law constant, A (MPa^{-n} s^{-1})	6.7×10^{-6}	6.3×10^{-2}	7×10^3	6.8×10^3	7×10^3
Creep activation energy, E (kJ mol^{-1})	156	276	520	276	510
Power law constant, n	2.4	3.05	3	4	3

Experiment	Erosion coefficient k_e (m^2 yr^{-1})	Extension velocity (cm yr^{-1})	Weak zone dip degrees	Lithospheric, crustal thickness (km)	Moho temperature (°C)
M1	500	−0.65 + 1.35	50	150, 48	740
Mf	500	−1 + 2	50	150, 48	740
Mf2	500	−1.33 + 2.66	50	150, 48	740
Ms	500	−0.5 + 1	50	150, 48	740
Mst	500	−0.5 + 1	50	135, 40	725
Mt	500	−0.65 + 1.35	50	135, 40	725
Mft	500	−1 + 2	50	135, 40	725
Mft2	500	−1.33 + 2.66	50	135, 40	725
M1le	250	−0.65 + 1.35	50	150, 48	740
M1he	750	−0.65 + 1.35	50	150, 48	740
M1ne	0	−0.65 + 1.35	50	150, 48	740
Mws	500	−0.65 + 1.35	65	150, 48	740
Mwg	500	−0.65 + 1.35	30	150, 48	740
Mwr	500	−0.65 + 1.35	−50	150, 48	740
Mwv	500	−0.65 + 1.35	90	150, 48	740
Mtp	500	−0.65 + 1.35	–	150, 48	740
Mo	500	−0.65 + 1.35	50	150, 48	585

The thermo-mechanical properties of each element of the numerical grid are defined by the temperature and pressure dependent density, the thermal and elasto-visco-plastic parameters of its material. An initial overthickened and thermally weakened orogenic lithosphere is simulated by a crustal thickness of 40–48 km at Moho temperatures of 725–740 °C and lithospheric thickness variable between 135–150 km (Fig. 1). The initial thermal structure of the lithosphere is averaged from available observations in young orogens with 0 °C on the surface and 1330 °C at the base of the lithosphere (Fig. 1). Moho temperatures of ∼740 °C are generally observed in young orogenic settings (Tesauro et al., 2009). Our chosen rheological and thermal parameters are limited to one type that averages a typical young and hot orogen (Fig. 1, and Table 1) where rheological decoupling of the crustal and lithospheric layers takes place in most cases and results in horizontal ductile flow in the intermediate or lower crust (Burov, 2011). In such a decoupled "jelly sandwich" type of rheology, the strength of the lithospheric mantle is especially weak due to the high temperature values. We have not implemented variable rheologies in our extensional model because their role is extensively discussed elsewhere (Burov and Poliakov, 2001; Burov, 2011).

Furthermore, a 15 km thick rheological weakness zone simulating an inherited subduction/suture zone or major lithospheric-scale thrust contact has been implemented in the centre of our models by decreasing the creep activation energy. This type of implementation is commonly successfully used in modelling to simulate rheological weakness zones (e.g., Li et al., 2011; Liao and Gerya, 2014; Sokoutis et al., 2007). We assume that the former subduction and subsequent collision phase have resulted in a thickened crust and a weak suture zone in the mantle (Fig. 1). The latter is attributed to fluids released during subduction, which causes a major rheological contrast in the mantle. While in nature series of thrusts are distributed over a larger area, their size and rheological contrast are less effective at our given resolution (Burg and Gerya, 2005). The angle of dip of the rheological weak zone has been tested in a number of models as a parameter influencing the geometry of extension (Fig. 1). These experiments were also compared with one model without any weakness zone, where strain localisation occurred by an initial thermal anomaly of +50 °C at the base of the lithospheric mantle at the beginning of the experiment. The implemented viscosity fields of our models are shown in Appendix A. A model with stronger coupling between the crust and lithospheric mantle is shown in Appendix A. Further details are available in Appendix B and previous publications using this numerical approach (e.g., Burov and Poliakov, 2001; Francois et al., 2013).

Divergent velocities on the sides of the model during the syn-rift phase simulate extension. Starting from the reference model, different lateral velocities were tested in subsequent models (Table 1). When studying the effects of the extensional velocity, experiments with initial thicker lithosphere (150 km) were compared after the same amount of 240 km total extension. Models with a thinner configuration (initial crustal thickness of 40 km, lithospheric thickness of 135 km) were analysed when the same amount of lithospheric thinning was obtained compared to the thicker scenarios. The overall values of total horizontal extension, extensional velocities and duration of syn- and post-rift basin evolution are taken from averages from observed values in Mediter-

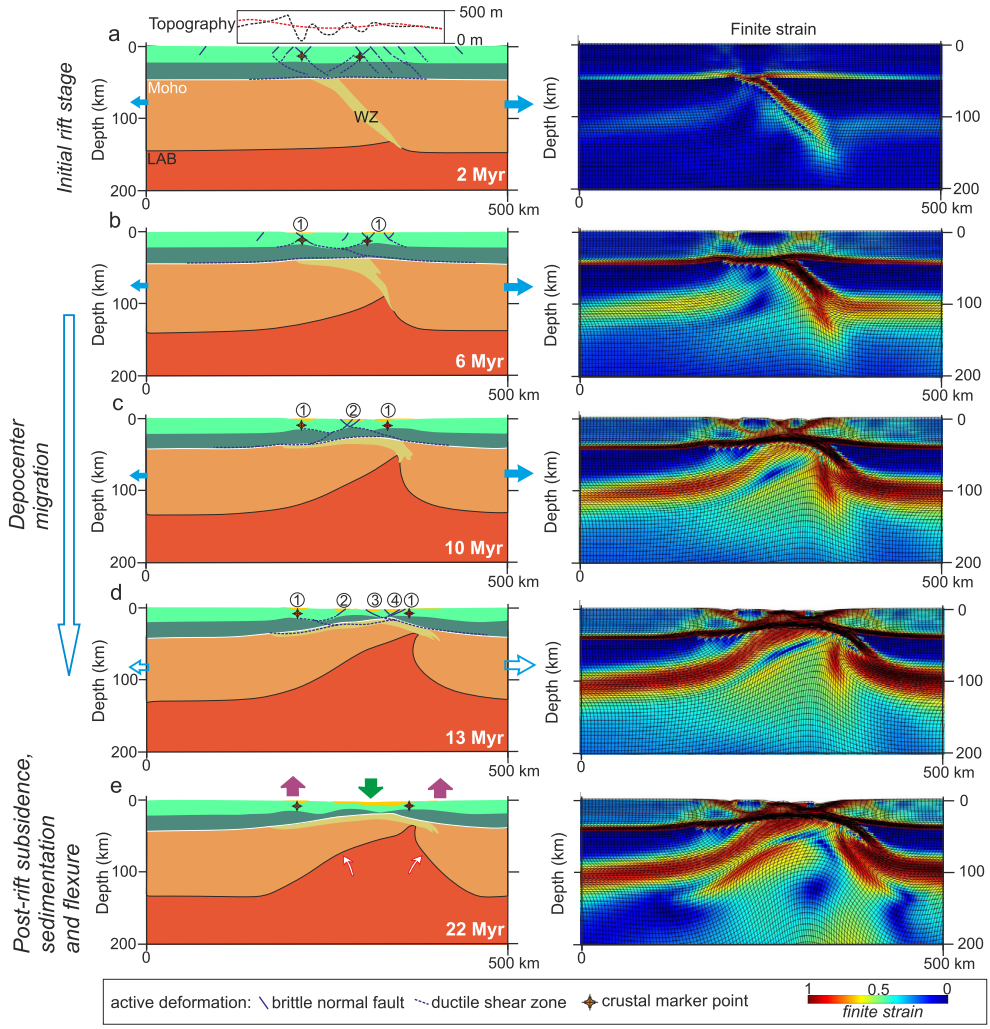

Fig. 2. Evolutionary model of the reference experiment (M1 in Table 1). Model results are illustrated by lithospheric layering geometries (i.e., phase configuration: upper crust, lower crust, lithospheric mantle and the underlying asthenosphere, yellow colour represents sedimentary basin fill) on the left and finite strain on the right panels. Two crustal marker points are plotted on the phase configuration showing the evolution of extension with time. The inherited weakness zone (WZ) controls the fast lithospheric mantle attenuation, while the style of crustal thinning evolves from an initial stage (a) to a localised, migrating style (b–d). An initial central updoming results from the asthenospheric uprise (topography above 2a with and without erosion, red and black curves, respectively). During the post-rift evolution (d–e) lateral heat transport results in uplift (purple arrows), erosion of the basin margins and subsidence of the basin centre (green arrow). Faults and shear zones are indicated based on the calculated strain rate results of the thermo-mechanical models. Blue horizontal arrows show the asymmetric extension velocities imposed on the model sides for 13 Myr simulating back-arc extension and then the velocities are set to 0 for the post-rift phase (d–e). (For interpretation of the colours in this figure, the reader is referred to the web version of this article.)

ranean back-arc basins (Faccenna et al., 2014). Zero velocities are applied during the subsequent post-rift evolution. In order to simulate the back-arc character of the extension, we have implemented different extensional velocities at the sides of our model, where the velocity at one boundary is double the value than on the opposite side (Fig. 1). The higher velocity on one side of the model simulates the effect of slab retreat. Further subduction effects, such as slab sinking or slab related asthenospheric flows, are ignored to discriminate them from the studied extensional kinematics. Most of our model setups include a weak zone dipping in the opposite direction relative to the direction of subduction during slab-retreat simulated in our models (i.e. dipping to the right relative to the retreat of a slab dipping to the left in Fig. 1). Such a geometry is more often observed in nature due to the extensional reactivation of a contractional retro-wedge or back-arc.

3. Numerical modelling results

Starting from a reference model (Fig. 2) the influence of the extension velocities, erosion rates, the inclination of the rheological weak zone and the lithospheric/crustal thicknesses were tested and described in subsequent models (Figs. 3–7). Note that the same amount of bulk stretching in our models creates different amounts of crustal and lithospheric thinning as a function of strain localisation, surface processes and convective thermal erosion of the lithosphere. Model results are illustrated by lithospheric layering geometries (i.e. cross-section of phase configuration: upper crust, lower crust, lithospheric mantle and underlying asthenosphere), finite strain (Figs. 2–4) and temperature distribution (Fig. 6) at various times (Figs. 2, 6 and 7). A comparison of different models is shown in Figs. 3–5.

3.1. Reference model results

The reference model (M1, Fig. 2, Table 1) simulates the extension of an overthickened orogenic structure affected by typical rates of extension observed in the Mediterranean area. It has initial thicknesses of 24 and 24 km for the upper and lower crust, respectively, 740 °C Moho temperature and 150 km lithospheric thickness. An erosion coefficient of 500 $m^2\,yr^{-1}$ is applied dur-

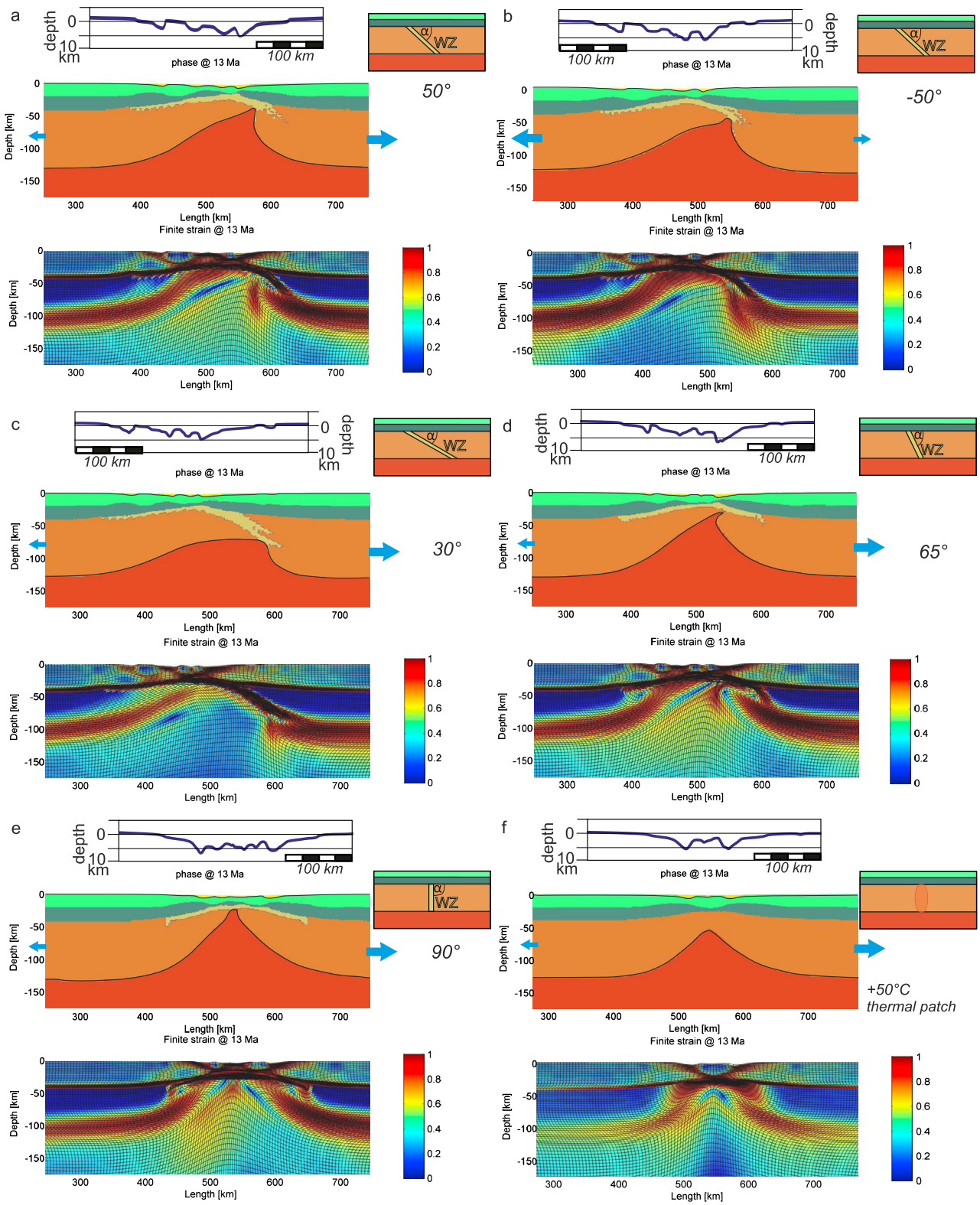

Fig. 3. The influence of the initial angle of dip and dip direction of the rheological weak zone (WZ). Upper panels: phase configuration after 13 Myr of extension and initial phase configuration (upper right); lower panel: finite strain result after 13 Myr of extension. Above the panels the basement depth profiles are drawn after 13 Myr of extension. a–f) models M1, Mwr, Mwg, Mws, Mwv, Mtp (Table 1), respectively. a) Reference model M1; b) The weak zone is dipping in the opposite direction compared to the maximum lateral velocity; c) Initial lower dipping angle of the rheological weak zone; d) Initial steeper dipping angle of the rheological weak zone; e) Initial vertical rheological weak zone; f) No weak zone, extension initiated by an initial thermal perturbation in the mantle lithosphere. Blue horizontal arrows show the asymmetric extension velocities of $-0.65 + 1.35\ \mathrm{cm\,yr^{-1}}$ imposed on the model sides. (For interpretation of the colours in this figure, the reader is referred to the web version of this article.)

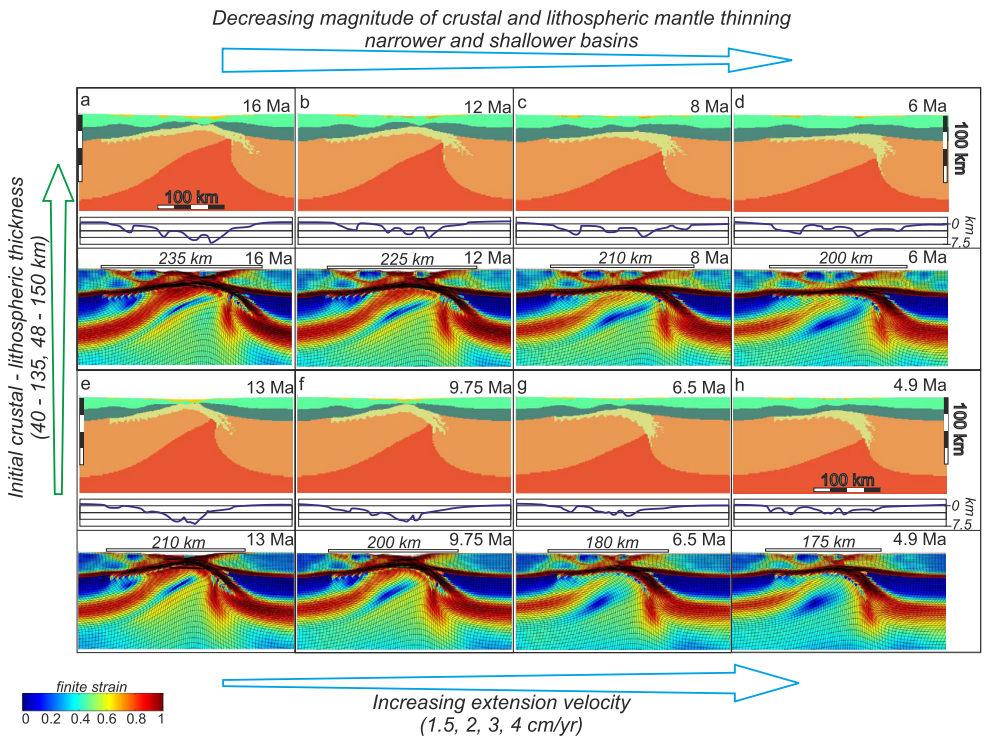

Fig. 4. Comparison of phase configuration (upper panel), basement subsidence (middle graph) and finite strain (lower panel) results of models with different extension velocities (1.5, 2, 3 and 4 cm/yr) and initial crustal/lithospheric thicknesses. (a–d) Ms, M1, Mf experiments with higher initial crustal and lithospheric thickness after 240 km of bulk extension; (e–h) Mst, Mt, Mft, Mft2 experiments with lower initial crustal and lithospheric thickness after 195 km of bulk extension. Bars above the finite strain panels show the final width of the area affected by extensional deformation.

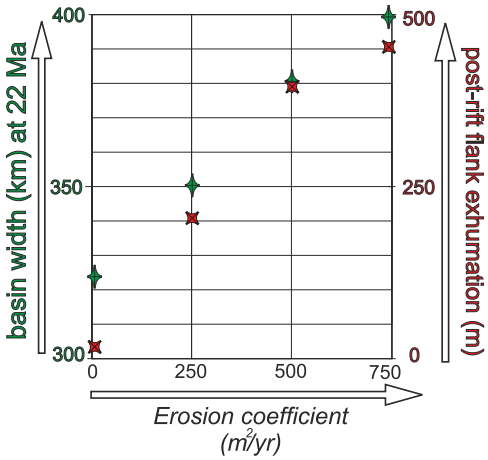

Fig. 5. Control of different erosion rate values on the width of the extensional basin (models M1ne, M1le, M1, M1he in Table 1). Post-rift exhumation of the basin margins increases with higher erosion rates. Green symbols show the basin width, red symbols show values of post-rift flank exhumation after 13 Myr of extension and additional 9 Myr of thermal cooling. (For interpretation of the colours in this figure, the reader is referred to the web version of this article.)

ing the 13 Myr of extension and the subsequent 9 Myr of post-rift evolution. An initial dip of the lithospheric weakness zone of 50° was defined.

During the first 2–3 Myr, the extensional geometry is controlled by fast lithospheric mantle thinning resulting in an initial updoming in the centre of the model with very shallow and restricted accommodation space (Fig. 2a). The crust is affected by low offset normal faulting when the underlying lithospheric mantle weakness zone is partly re-distributed over a larger area. This is followed by localisation of deformation, which creates deeper depocentres in individual half-grabens (1–4, Fig. 2). These sub-basins form at first near the margins of the underlying and progressively re-distributed weakness zone. Subsequently the extension migrates with time towards the centre of the area overlying the re-distributed weakness zone. Therefore, younger depocentres are located more to the centre of the extensional area between older sub-basins (from 1 to 4, Figs. 2b–d). The upper crustal thinning is accommodated by lower crustal ductile flow resulting in opposing thinning geometries (Fig. 2c). The rapid ascent of the asthenosphere is highly asymmetric, mirroring the localisation of extension along the partly re-distributed weakness zone. This localisation leads to migration of the newly formed sub-basins (direction of younging from 1 to 4 in Fig. 2d) that follows the initial dipping direction of the weakness zone. At the end of the syn-rift phase, the location where the crust records maximum thinning is horizontally offset (with ∼20 km) from the position showing the highest asthenospheric ascent. Domains of maximum and minimum thinning are opposed in the upper and lower crust.

After the extensional velocity reduces to zero, the thermal relaxation of the highly asymmetric asthenosphere uprise will be attenuated towards a more symmetric configuration due to lateral cooling. During this stage, the place recording maximum mantle lithospheric thinning is still horizontally offset from the location of the basin depocentre. The lateral heat transfer from the asthenospheric upwelling creates flexural uplift and erosion near the margin of the area affected by crustal extension. Sediments are re-deposited in the centre of the basin. This re-distribution results in flexure of the thermally weakened lithosphere, which enhances differential vertical movements and creates minor upper crustal deformation and lower crustal flow (see also Burov and Poliakov, 2001).

3.2. Parameter sensitivity study

The effect of the initial dipping angle and dip direction of the rheologically weak zone was tested in a series of experiments, il-

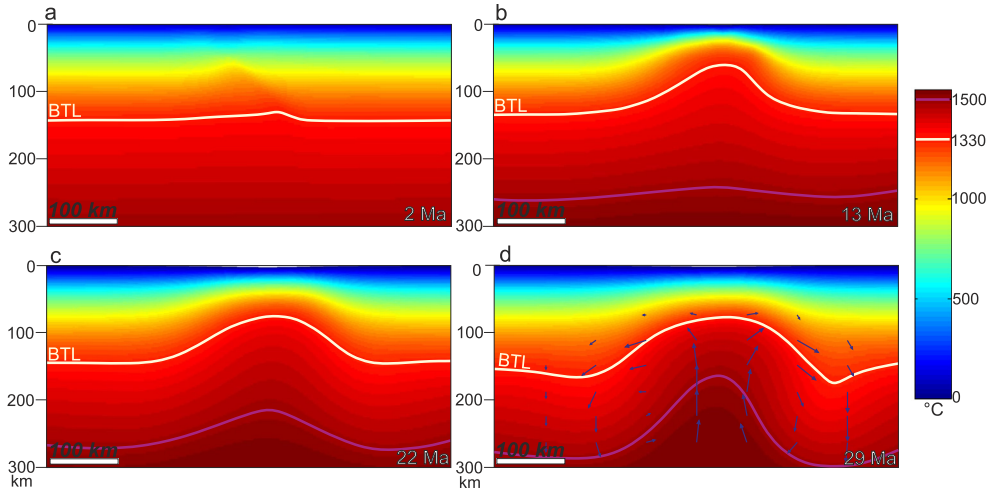

Fig. 6. Thermal evolution of the reference model M1. a) After 2 Ma; b) at the end of the 13 Ma syn-rift extension; c) after 9 Myr of post-rift evolution. The conductive thermal cooling is associated with subsidence of the basin centre. The asthenospheric thermal anomaly is wider due to lateral heat transport; d) after 16 Myr of post-rift evolution. A convective upwelling of the deep asthenosphere and drip-off of the marginal mantle lithosphere are observed. BTL – base of the thermal lithosphere, purple line – 1500 °C isotherm, blue arrows indicate the velocity field. (For interpretation of the colours in this figure, the reader is referred to the web version of this article.)

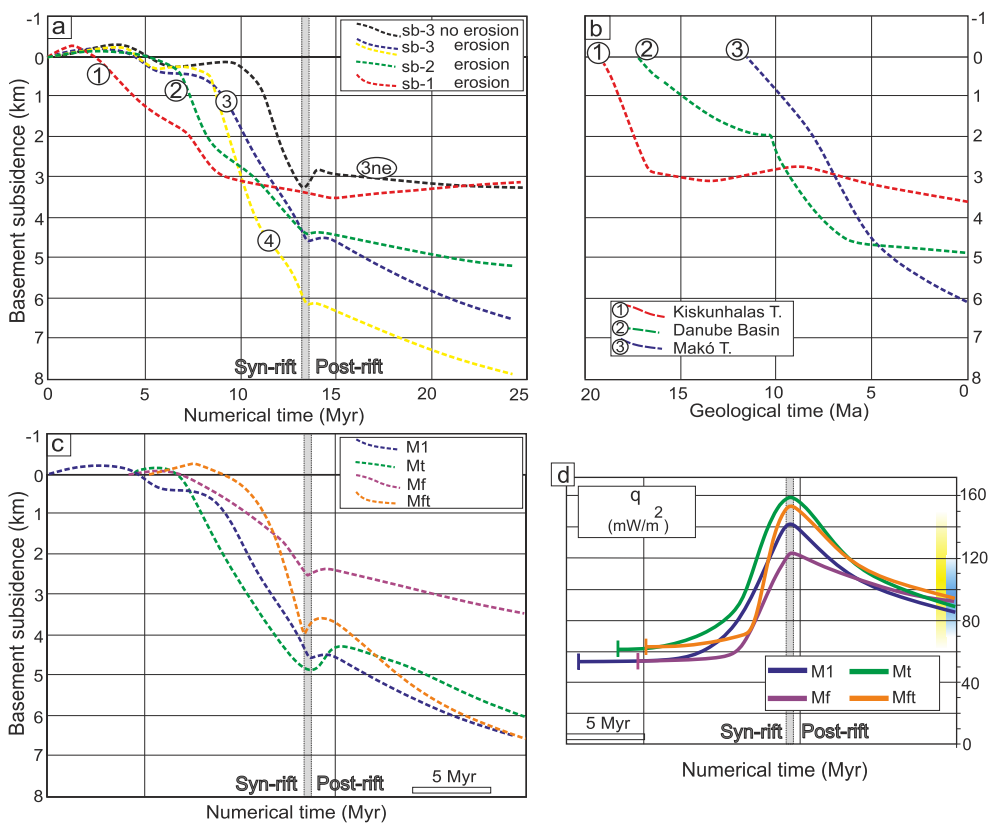

Fig. 7. (a) Predicted basement subsidence curves from different locations of the reference model M1. Curves correspond to various sub-basins (1–4), as marked in Fig. 2. Black curve shows the subsidence of sub-basin 3, but without any erosion applied during the modelling (model M1ne, Table 1); b) Reconstructed basement subsidence history of sub-basins from the Pannonian basin system (modified after Balázs et al., 2016). Peak of syn-rift subsidence varies from Early, Middle to Late Miocene in the Kiskunhalas, Danube and Makó basins, resp. (c) Basement subsidence curves of different modelling scenarios from the central part of the experiments. (d) Surface heat flow evolution of thick lithospheric models with 260 km of extension, thinner lithosphere models with 195 km extension. Mf – model with higher extension velocity. Mt – model with thinner initial lithospheric thickness. Mft – model with higher extension velocity and thinner initial lithosphere. Blue and yellow signs at 0 Ma show the present day surface heat flow values of the Pannonian and Aegean basins, respectively (after Lenkey et al., 2002; van Wees et al., 2009). Grey line on various panels indicates the end of the syn-rift period. (For interpretation of the colours in this figure, the reader is referred to the web version of this article.)

lustrated at the end of the syn-rift phase (Fig. 3). We have tested four dip angles in the direction of the maximum lateral velocity (30°, reference model of 50°, 65° and vertical, Figs. 3a,c,d,e) and one with opposite direction (−50°, Fig. 3b). We have compared these results with a model where no tilted rheological weakness zone was present, but strain localisation was achieved by inserting a rectangular seed of 10 times 10 km at the base of the lithosphere in the centre of the model where the temperature is +50 °C higher than the surrounding rocks (Fig. 3f). This thermal seed weakens the overlying lithosphere and localises the strain. When the dip of the weak zone is opposite to the direction of the maximum lateral velocity (Fig. 3b), the lithosphere is less thinned but the width of the asthenospheric anomaly and overlying sedimentary basin is higher. In this situation, the horizontal offset between the locations of maximum crustal and lithospheric mantle thinning is higher when compared to the reference model (Figs. 3a,b). The edge of the asthenospheric anomaly is still steeper in the initial dip direction of the rheological weak zone, implying a stronger control of the dip direction compared with the direction of maximum lateral velocity. Testing the influence of the dip angle of the rheological weakness zone (Figs. 3a,c–e) shows that a steeper weak zone creates a more symmetric asthenospheric uprise, higher crustal and lithospheric thinning, narrower and deeper overlying sedimentary basins and lower horizontal offset between the locations of maximum crustal and mantle thinning. When the weak zone is vertical (Fig. 3e), the model shows a more pronounced lithospheric mantle thinning when compared with models without a weak zone (Figs. 3e,f see also Burov and Poliakov, 2001), and a symmetric final lithospheric geometry structure and overlying sedimentary basin. In the model without a weak zone (Fig. 3f), the overall narrower sedimentary basin is composed of two localised depocentres that formed in the same manner and at the same time, and symmetrically overlies a significantly lower asthenospheric uprise, when compared with models containing a tilted weak zone.

The effect of different extension velocities was tested by comparing experiments with different extensional velocities (sum of the left and right side of the experiment) of 1.5, 2, 3, 4 cm/yr (Fig. 4, Table 1) and with different crustal and lithospheric thicknesses (40 and 48 km, 135 and 150 km, Figs. 4a–d and Figs. 4e–h, respectively). We compare our results in such a way that the amount of lithospheric thinning is constant (at bulk extension of 195 and 240 km, respectively). All other parameters were kept constant relative to the reference model. In all experiments the right boundary velocity is double the value than on the left side. The experiments show that increasing the extensional velocity, and thus decreasing the modelled time duration, results in decreased asthenospheric uprise and lower amounts of crustal thinning, creating a narrower and shallower overlying sedimentary basin in both lithospheric thickness configurations (Fig. 4). For instance, in the models with an initial lithospheric thickness of 150 km, the width of the crustal deformed zone decreases from 235 km to 200 km when comparing models with extension velocities of 1.5 cm/yr and 4 cm/yr, respectively (Figs. 4a,d). A similar decrease from 210 km to 175 km is observed in models with a lower initial lithospheric thickness (Figs. 4e,h). Our models show that the crustal/lithospheric thinning and width of the overlying sedimentary basin is not only controlled by the amount of extension, but also by the rate of extension.

For the two initial lithospheric configurations (crustal thickness 40 and 48 km, lithospheric thickness 135 and 150 km, Figs. 4a–d and Figs. 4e–h, respectively) the final width of the sedimentary basin can be as large as the previously thickened crustal domain amplified by the amount of bulk extension (Brun, 1999). Obviously, experiments with higher initial crustal and lithospheric thickness require a larger amount of total extension in order to create similar crustal and lithospheric thickness values underlying the sedimentary basin when compared with initially thinner crust and lithosphere models (240 km versus 195 km total extension, respectively, Fig. 4). Hence, models with a thicker initial lithosphere create wider asthenospheric upwelling and overlying sedimentary basins.

The effect of surface processes has been simulated by testing variable erosional rates in our models. Four erosional coefficients have been tested by our models (0, 250, 500, 750 $m^2\,yr^{-1}$, Fig. 5, Table 1). The experiments infer that the final width of the overlying sedimentary basin at the end of the model runs (syn- and post-rift period) increases with increasing erosion rate (i.e., from 315 km for zero erosion to 400 km for an erosion coefficient of 750 $m^2\,yr^{-1}$, Fig. 5). This is related to the erosion of the flanks and an additional sediment loading in the basin centre, in agreement with previous studies (e.g., Burov and Poliakov, 2001). Therefore, a high rate of erosion enhances exhumation of the basin margins.

4. Inferences from thermo-mechanical modelling

The implementation of a rheological weak zone in the mantle lithosphere drives an asymmetric evolution of the extensional system. A number of features are similar to findings by previous modelling studies, where the initiation of the rifting is induced by symmetrical weak seeds or thermal perturbations (e.g., Huismans and Beaumont, 2003). However, the asymmetry of our model enhances some of the known effects and creates novel patterns that require interpretations.

4.1. Lithospheric-scale thermal evolution

Our numerical models show a similar large scale convective behaviour created by the interaction between the asthenosphere and mantle lithosphere as inferred previously (Huismans et al., 2001; Burov, 2007; Cloetingh et al., 2013; Burov and Gerya, 2014). The convective upwelling of the asthenosphere and lateral down welling of the mantle lithosphere is accentuated in our models because of the large amounts of extension combined with the initial thick, hot and weak orogenic lithosphere (Fig. 6). The ultimate geometry of the asthenospheric upwelling (Huismans et al., 2001) and associated surface heat flow is a combination between convective and conductive heat transport effects. The continuation of convection results in plume head interactions, where deep asthenosphere ascent is accommodated by lateral down welling and drip-off of lithospheric mantle (Cloetingh et al., 2013). Furthermore, our models predict the novel possibility of a switch between thermal cooling and asthenospheric uprise during post-rift times: this is observed in the thermal evolution of the reference model (Fig. 6), where an initial post-rift cooling of the lithosphere-asthenosphere boundary (Fig. 6b) is followed by its ascent again due to deeper asthenospheric uprise, the latter being visible, for instance, in the 1500 °C isotherm (Figs. 6b–d).

Such convective processes also control the correlation between an increase of the extensional velocity and a decrease of both lithospheric thinning and overlying sedimentary basin width (Fig. 4). The convective thermal erosion has a higher impact in models with lower extension rates, when there is more time to grow thermal instabilities. This is in accordance with the results of Burov (2007), who showed that positive Rayleigh–Taylor instabilities results in faster lithospheric thinning in experiments with lower extension velocities after the same amount of extension. The convective heat transport in the asthenosphere is much more effective than the conductive heat transport in the crust and associated heat loss. The accentuation of asthenospheric uprise by convection during slower extension decreases the lithospheric strength over a larger area, distributing the crustal thinning and, therefore, increasing the width of the basin. The viscosity of the

ductile layers is exponentially dependent on the temperature and therefore the active upwelling of the lithosphere–asthenosphere boundary has a higher impact in such cases than the strain rate variation. In other words, the thinning of the lithosphere is the joint result of the passive extension controlled stretching and the active upwelling of the hot asthenosphere. This is controlled by thermal effects and it is in contrast with analogue modelling inferences. Although analogue model experiments are especially suitable in general for studying 3D fault geometries (Corti et al., 2003 and references therein), it should be noted that temperature evolution is not implemented in such models.

4.2. Sedimentary basin evolution

The evolution of the topography during extension indicates a generalised uplift during the initial extension, combined at higher resolution with the formation of footwall uplifted and hanging-wall subsided areas (Fig. 2a). This is similar to many other active extension systems, both in nature and in experiments (e.g., Ziegler and Cloetingh, 2004; Corti et al., 2003 and references therein). Specific for our models is the topographic asymmetry created by larger differential vertical movements in opposite direction when compared with the dip of the rheological weak zone.

Our asymmetric models are characterised by a lateral migration of depocentres during the syn-rift phase in the sedimentary basin (Fig. 2). At the end of this syn-rift period, the oldest basins are located near the margins of the extensional basin system, with the youngest basin located more to the centre in an asymmetric position, closer to the margin overlying the maximum asthenospheric uprise. This migration is controlled by the evolution of the rheologically weak zone that is gradually redistributed and elongated in a continuous sub-horizontal layer in the upper part of the lithospheric mantle. This weak layer provides an effective decoupling, enhancing the weakening effect of the asthenospheric uprise and focuses deformation. The formation and evolution of the overlying sedimentary basins are limited to the area where this layer is present at depth. While thinning is continuously focused in the weak layer of the mantle lithosphere accentuating the asymmetry during the syn-rift time, the overlying crust records distributed deformation on a much larger area. The interplay between convective and conductive processes decreases the lithospheric mantle asymmetry during post-rift times and makes it more difficult to detect at longer times after extension has ceased. Our models show a change in crustal deformation mechanics during extension. The initial extension creates half-grabens associated with footwall uplift due to the steep orientation of the rheological weak zone, favouring the initiation of large scale detachments (Fig. 2, strain panels). The later re-orientation of the rheological weak zone to a sub-horizontal position favours more symmetric crustal deformation, where the formation of grabens is recorded.

Following the coordinates and thermal properties of marker points in the upper crust and overlying sediments we extracted the basement subsidence and surface heat flow history of our models and compared with constructed ones from the Pannonian basin (Fig. 7). Analysis of the modelled subsidence patterns for the overlying sedimentary basin indicates that in all cases an early moderate syn-rift subsidence stage is subsequently followed by periods of fast syn-rift subsidence, stagnation or uplift (Fig. 7a). Such variability is obviously controlled by different degrees of crustal and lithospheric mantle thinning combined with associated thermal effects. The thermal evolution of the sedimentary basins is strongly coupled with the time duration of extension. Fast extension models predict a maximum surface heat flow that is $\sim$20 mW/m^2 lower in the most extended crustal area, when compared with the reference model (Fig. 7d, Mf, M1). A similar pattern is observed in models with lower lithospheric thickness (Fig. 7d, Mt, Mft). All models containing a weakness zone predict larger amounts of lithospheric thinning when compared with models where such a zone is absent (Fig. 3). It also demonstrates that local zones of extreme thinning in the lithospheric mantle can be obtained rather by extension than attributing them to local or external mantle plumes.

A significant uplift at the onset of the post-rift evolution is created by the rapid cessation of extension at the transition between syn- to post-rift, which simulates the transition from rapid roll-back to collision and slab-detachment affecting extensional back-arcs. Such a rapid cessation of extension works against the rift push forces still affecting the lithospheric mantle (e.g., Huismans et al., 2001) and the ductile flow of the lower crust due to gravitational loading differences (Burov and Poliakov, 2001). This creates a short lived inversion that induces uplift in the order of few tens to hundreds metres in the centre of the basin as observed in different model setups (Figs. 7a,c). The subsequent post-rift subsidence rates are dependent on the inherited crustal/lithospheric thinning and the rate of surface erosion active during both the syn- and post-rift times (Figs. 5, 7a,c). We have implemented a simplistic 2D sedimentary transport route from the uplifted and eroded footwalls towards the basin centre. This is coupled with the flexural (un)loading of a thermally weakened lithosphere, which is further enhanced by the re-distribution of the weak zone. The overall spatial and temporal migration of depocentres in our asymmetric model combined with surface processes and lateral heat transport induces uplift and erosion reaching 400 m near the basin margins during post-rift times (Fig. 5). High resolution 3D morphological models can specify the detailed patterns of landscape evolution (e.g., Ellis et al., 1999).

5. Comparison with observations from extensional back-arc basins

We compare our numerical modelling results with observations in extensional back-arc basins formed in the hinterland of highly arcuated Mediterranean orogens that formed in response to the rapid retreat of a number of genetically associated slabs (e.g., Faccenna et al., 2014). The Pannonian, Aegean, Alboran, Liguro-Provencal–Thyrrenian and Black Sea extensional back-arc basins formed in response to the rapid retreat of the Vrancea, Aegean, Gibraltar, Calabrian and Neotethys slabs during the formation of the Carpathians, Hellenides, Betics-Rif, Apennines and Turkey–Cyprus orogenic areas, respectively (e.g., Wortel and Spakman, 2000; Faccenna et al., 2014). The most suitable correlation with our modelling are the thinned continental extensional back-arcs of the Pannonian and Aegean basins, where the Paleogene–Miocene extension has affected an inherited Alps, Carpathians, Dinarides and Hellenides orogenic nappe stack by reactivating primarily the inherited Neotethys/Vardar and/or Pindos suture zones (e.g., Jolivet et al., 2013; Matenco and Radivojević, 2012).

5.1. The Pannonian Basin system

The orogenic area presently underlying the Miocene Pannonian basin (Fig. 8) formed in response to the opening and closure of the Alpine Tethys and a northern branch of the Neotethys oceans. While the Neotethys branch opened during Middle Triassic and was closed by successive moments of late Jurassic–Cretaceous subduction and continental collision, the Alpine Tethys opened during the Middle Jurassic and was subsequently closed by successive moments of Cretaceous–Miocene shortening observed at the exterior of the Carpathians (e.g., Schmid et al., 2008 and references therein). Towards the end of the Paleogene times these movements have created a large orogenic area with thickened crustal structure and composed of two main tectonic megaunits, i.e., ALCAPA and Tisza-Dacia (Fig. 8). While their contact is thought to have

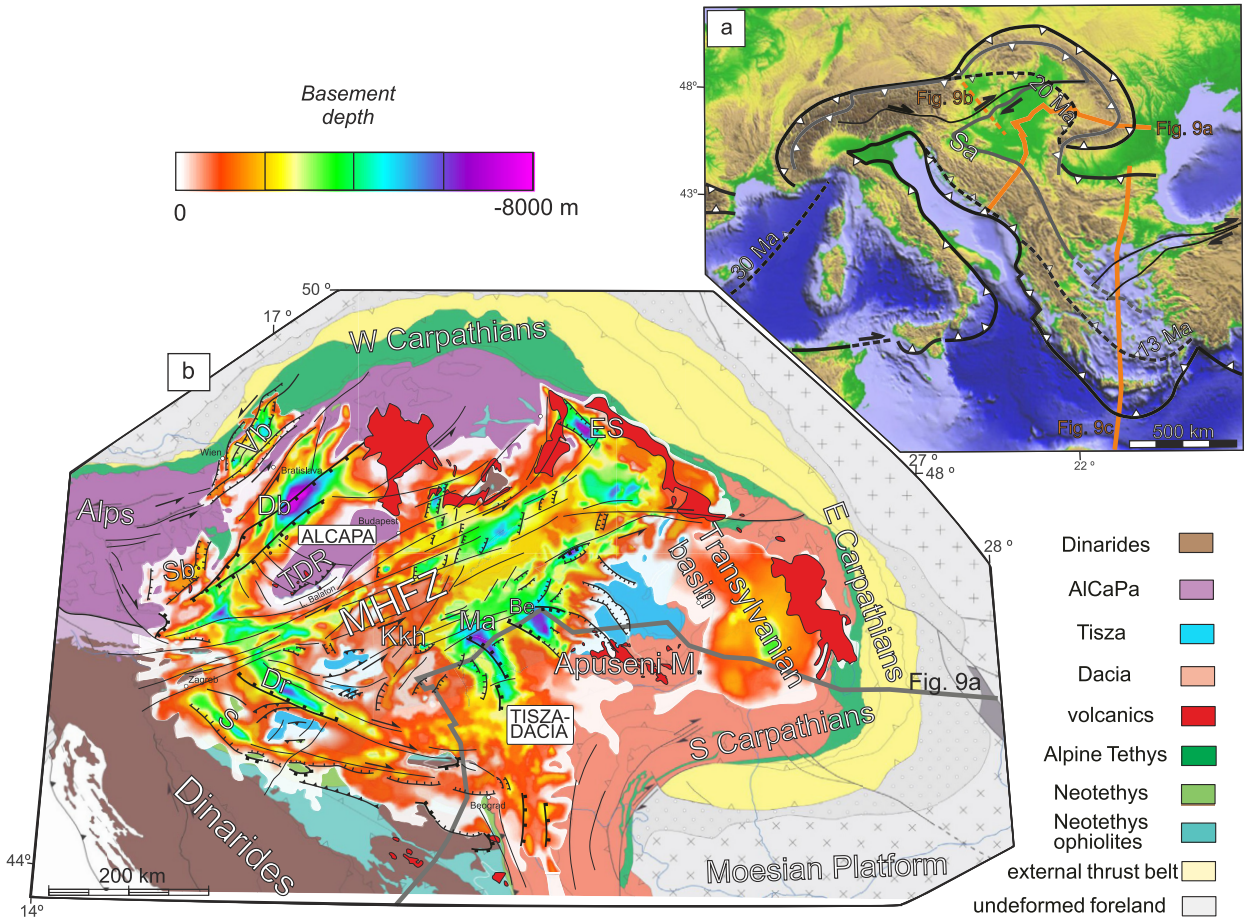

Fig. 8. (a) Simplified tectonic outlines of plate contacts in the Mediterranean region (after Schmid et al., 2008; Faccenna et al., 2014). Dashed black lines show the positions of the orogenic front prior to the onset of extension in back-arc basins (modified after Wortel and Spakman, 2000). Sa – Sava Suture Zone. (b) Simplified tectonic map of the Alps – Carpathians Dinarides region (modified after Schmid et al., 2008) overlain by the Miocene – Quaternary sedimentary thickness (in meters) of the Vienna (Vb), Pannonian and Transylvanian basins. MHFZ – Mid Hungarian Fault Zone, Db – Danube basin, TDR – Trans-Danubian Range, Sb – Styrian basin, ES – East Slovak basin, Dr – Drava Trough, S – Sava Trough, Kkh – Kiskunhalas subbasin, Ma – Makó Trough, Be – Békés basin.

been a large transcurrent fault zone accommodating the change in polarity between the Carpathians and the Dinarides, the Tisza-Dacia unit was largely sutured over the Dinarides during Latest Cretaceous times along the Sava Suture Zone (Schmid et al., 2008; Ustaszewski et al., 2010). The overall orogenic area together with the inherited suture zones and nappe contact was subsequently affected by 220–270 km of Miocene extension that created the Pannonian Basin back-arc during the coeval N, NE- to E-ward retreat of a slab situated at the exterior of the Carpathians (Fig. 9a, e.g., Horváth et al., 2015). The extension ceased rapidly during the final stages of the 13–8 Ma Middle–Late Miocene collision of the Carpathians (e.g., Matenco et al., 2016). The present structure indicates maximum crustal and lithospheric thinning to 20–22 km and 50–60 km (Fig. 9a), respectively, with evidence for large scale shearing and serpentinisation in the mantle lithosphere (Posgay et al., 2006; Hetényi et al., 2015; Lenkey et al., 2002; Horváth et al., 2015).

Kinematic and exhumation studies have demonstrated that the subsidence in half grabens in the large Great Hungarian Plain part of the Pannonian Basin (Tari et al., 1999) was associated with significant exhumation of the Dinaridic orogenic margin, controlled by extensional detachments that largely reactivated the inherited Sava Suture Zone contact with the Tisza-Dacia unit (Fig. 9a, e.g., Ustaszewski et al., 2010). In agreement with our reference numerical model this suture zone is dipping NE-wards at the Dinaridic basin margin near the Sava Trough, similarly with the main direction of the roll-back of the Carpathian slab. In agreement with our numerical modelling results, this extension migrated in space and time during the Miocene from Early Miocene near the basin margins to maximum ∼7 km deep Late Miocene structures (Figs. 7b and 9a) situated asymmetrically towards the SE margin of the basin (Balázs et al., 2016). Our modelling infers a large spatial shift between the crustal location of the Sava suture zone and its equivalent in the lithospheric mantle and is in agreement with the observation of opposed maximum and minimum thinning in the upper and lower crust (Fig. 9b, see also Hetényi et al., 2015). Modelled subsidence patterns are in agreement with observations in the basin during the migration of deformation (Figs. 7a and b). More specific, sub-basins like the Styrian, Sava or East Slovakian basin situated near the margins of the area have rapid initial Early–Middle Miocene subsidence followed by stagnation or uplift, while later Middle–Late Miocene basins show a gradual acceleration during late-syn to post-rift times. The widespread unconformity recorded near the transition between the Middle and Late Miocene in the centre of the Pannonian Basin (Balázs et al., 2016) is generally attributed to a short-lived inversion triggered by the Carpathian collision (Horváth, 1995). A similar observation in our modelling near the transition between syn- to post-rift times implies that such uplift could also be driven by the rapid cessation of the extensional forces. The extension and subsequent thermal subsidence in the Pannonian Basin was followed by a period of inversion (Bada et al., 2007) characterised by shortening and uplift of

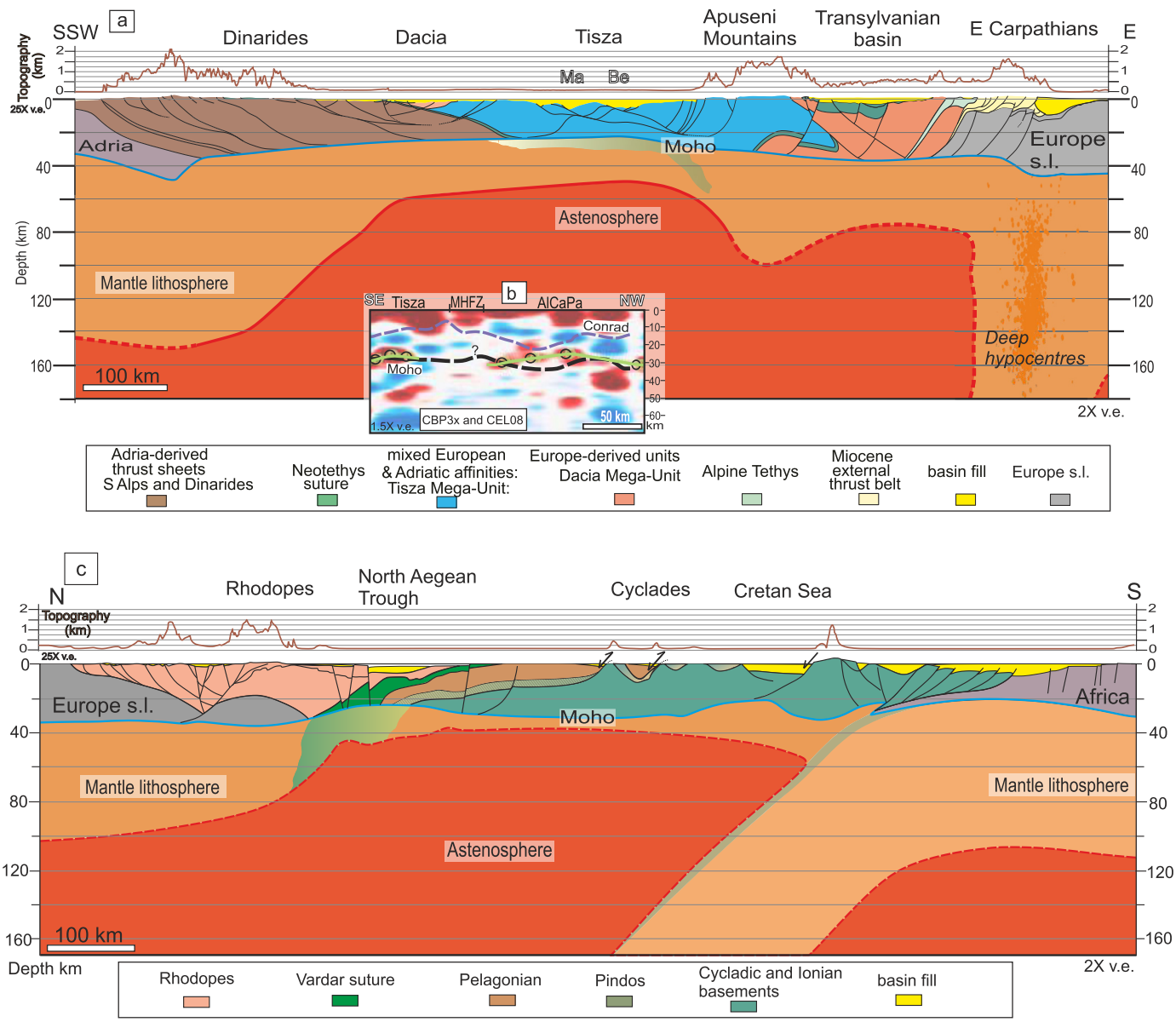

Fig. 9. (a) Lithospheric scale cross-section over the Dinarides–Pannonian Basin–Apuseni Mountains–Transylvanian Basin–East Carpathians (compiled from Schmid et al., 2008; Balázs et al., 2016; Matenco et al., 2016). The trace of the cross section (Fig. 8) was chosen to approximate the curved N to NE to E direction of extension accompanying the clockwise rotation of the Tisza-Dacia unit; b) Receiver function section over the Pannonian basin (from Hetényi et al., 2015). Green line shows the interpreted Moho, while purple and green lines show the interpreted Conrad and Moho surfaces based on the CEL08 deep seismic profile (Kiss, 2009). c) Cross section over Balkans–Rhodope–Aegean Sea–North Africa (modified after Jolivet and Brun, 2010; Menant et al., 2016) showing the crustal and lithospheric architecture of the Aegean–Rhodope extensional system. Location of the cross section is given in Fig. 8a. (For interpretation of the colours in this figure, the reader is referred to the web version of this article.)

the Dinarides margins and subsidence in the basin centre (Horváth, 1995; Horváth et al., 2015 and references therein). The similarity with modelling predictions (i.e., uplift over the basin margins and subsidence in its centre during post-rift times) implies that such differential vertical movements can also be accentuated by the evolution of the extensional thermal anomaly and surface processes, combined with flexural effects of the weak Pannonian lithosphere. Large asthenospheric ascent during extension favours the onset of genetically related magmatism. The post-Miocene mafic alkaline magmatism of the Pannonian Basin is not located at the syn- to post-rift transition, but culminates with larger volumes during the onset of Pliocene times (Kovács et al., 2012; Harangi et al., 2014). Such a late stage post-rift magmatic peak can be explained by the switch between thermal cooling and deeper asthenospheric ascent during post-rift times predicted by our numerical models (Fig. 6, see also Huismans et al., 2001).

5.2. The Aegean system

The Hellenides domain presently underlying the Eocene to present Rhodope–Aegean extensional system formed in response to the Middle-Late Triassic opening of the Vardar/Neotethys ocean and Pindos–Cukali–Budva thinned continental to oceanic domain followed by their subsequent and gradual Cretaceous–Eocene closure, continental collision and post-dating thrusting (Jolivet and Brun, 2010; van Hinsbergen and Schmid, 2012). These studies have suggested that the 400–600 km of back-arc extension accommodating the rapid retreat of the Aegean slab started during Eocene times with the formation of the Rhodope system of detachments and associated large scale exhumation and deformation gradually migrated southward, resulting in asymmetric extension in the Cyclades, Corinth Gulf and Crete. This was associated with major exhumation in the footwall of detachments combined with open-

ing of the Aegean Miocene basins, still active today (e.g., Brun and Sokoutis, 2007; Jolivet and Brun, 2010). Significant research has been dedicated to understanding the rheology and crustal coupling effects in the Aegean system (Jolivet et al., 2013 and references therein) and all studies agree on the strong localisation of deformation, largely reactivating the inherited Vardar, Pindos and related nappe contacts (Figs. 8a and 9d, see also Brun and Faccenna, 2008; Huet et al., 2011 and references therein).

The above findings suggest that the asymmetric back-arc modelling approach of our study is partly applicable to the Aegean extension, although the extension lasted longer, had higher amplitudes and there is no real rapid cessation during a post-rift period. Our modelling is in agreement with the earlier stages of Eocene–Miocene extension (see also van Hinsbergen and Schmid, 2012) and suggests that the extensional geometry was primarily controlled by the lithospheric mantle rheological weakness of the Vardar and/or Pindos suture zones. The redistribution of this weakness zone in the upper part of the lithospheric mantle may have induced the gradual migration of extension southward. In other words, not only the currently strongly debated Aegean crustal rheological strain localisation and the deep mantle forcing effects (see discussion in Jolivet et al., 2013) have a major impact during extension, but also the re-distribution of the inherited weakness zone in the upper part of the mantle lithosphere may condition the kinematics and geometry of Aegean extension. The southward migration in time from the Eocene Rhodope margin to the Miocene North Aegean (e.g., Brun and Sokoutis, 2007) corresponds to our predicted migration towards the main suture zone and is in agreement with the overall reduction of asymmetric effects (amounts of exhumation against detachments versus basin subsidence) in time southward. The more S-ward migration towards the Cyclades, Gulf of Corinth and Crete (i.e. migration in time towards the margin of the basin) is not in agreement with our single weakness zone modelling predictions, but may be related to the gradual activation with time of other major weakness zones in the direction of slab retreat, such as the Pindos suture or related nappe contacts. Such a multiple distribution of weakness zones or dynamic slab-related asthenospheric flow had significant effects in the Aegean system (e.g., Menant et al., 2016).

6. Conclusions

Numerical experiments simulating back-arc asymmetric extension of an overthickened lithospheric structure by reactivating inherited orogenic contacts suggest that large scale weakness zones play a major role in syn- and post-rift basin evolution. Such zones can be significantly re-distributed at deep crustal and mantle lithospheric depths during deformation and localise strain and associated asthenospheric convective and conductive effects. Switches between generalised post-rift asthenospheric cooling to localised upwelling may explain the delayed onset of mafic alkaline magmatism as observed, for instance, in the Pannonian back-arc system. Large-scale asthenospheric asymmetries created during syn-rift deformation may be significantly attenuated by subsequent thermal processes during the post-rift phase, creating ultimately apparent symmetric lithospheric structures. This results in contrasting deep mantle geometries when compared with overlying differential vertical movements recorded by the crust and the sedimentary basins. This plays a critical role in the spatial and temporal migration of individual basin depocentres across the extensional system, leading to variable subsidence patterns similar to reconstructed subsidence histories in Mediterranean extensional back-arcs as the Pannonian basin and the Aegean system.

Our experiments show that a steeper rheological weak zone creates a more symmetric asthenospheric uprise, higher crustal and lithospheric thinning, narrower and deeper overlying sedimentary basins and lower horizontal offset between the locations of maximum crustal and mantle thinning. Modelling suggests that thermal effects of the convective asthenospheric upwelling are more important for slower extension and it decreases the overall lithospheric strength over a larger area, distributing the crustal thinning. Therefore, lower extension rate results in wider basins and higher surface heat flow values. Our modelling also infers periods of significant uplift near the basin margins, created during the post-rift lateral heat transport, and in the basin centre, after the rapid cessation of back-arc extension driven by orogenic collision. Such processes create unconformities and differential vertical movements, such as observed during the post-rift evolution of the Pannonian basin. The subsidence rates of individual sub-basins and uplift along their flanks during the syn- and post-rift periods are controlled by the initial geometry of the lithospheric weakness zone and by surface processes. Our models are also in agreement with recent observations of a direct correlation between uplift and erosion at the margins of the basin and increased sedimentation towards its centre due to flexural and lower crustal flow effects.

Acknowledgements

This study is dedicated to the memory of prof. Evgueni Burov. The study was financed by the Netherlands Centre for Integrated Solid Earth Science (ISES) and Eötvös Loránd University, Budapest. We thank Jie Liao, Vincent Strak and an anonymous reviewer for their detailed and constructive reviews. László Lenkey is acknowledged for discussions on the thermal and tectonic evolution of extensional basins. Ferenc Horváth and László Fodor are thanked for their support and discussions about the Pannonian basin. The data supporting this paper are available by contacting the corresponding author.

Appendix. Supplementary material

Supplementary material related to this article can be found online at http://dx.doi.org/10.1016/j.epsl.2017.01.015.

References

Bada, G., Horváth, F., Dövényi, P., Szafián, P., Windhoffer, G., Cloetingh, S., 2007. Present-day stress field and tectonic inversion in the Pannonian Basin. Glob. Planet. Change 58, 165–180. http://dx.doi.org/10.1016/j.gloplacha.2007.01.007.

Balázs, A., Matenco, L., Magyar, I., Horváth, F., Cloetingh, S., 2016. The link between tectonics and sedimentation in back-arc basins: new genetic constraints from the analysis of the Pannonian Basin. Tectonics 35, 1526–1559. http://dx.doi.org/10.1002/2015TC004109.

Brun, J.-P., 1999. Narrow rifts versus wide rifts: inferences for the mechanics of rifting from laboratory experiments. Philos. Trans. R. Soc. Lond. 357, 695–710.

Brun, J.P., Sokoutis, D., 2007. Kinematics of the southern Rhodope core complex (north Greece). Int. J. Earth Sci. 96, 1079–1099. http://dx.doi.org/10.1007/s00531-007-0174-2.

Brun, J.P., Faccenna, C., 2008. Exhumation of high-pressure rocks driven by slab rollback. Earth Planet. Sci. Lett. 272, 1–7. http://dx.doi.org/10.1016/j.epsl.2008.02.038.

Brune, S., Heine, C., Perez-Gussinye, M., Sobolev, S.V., 2014. Rift migration explains continental margin asymmetry and crustal hyper-extension. Nat. Commun. 5. http://dx.doi.org/10.1038/ncomms5014.

Burg, J.-P., Gerya, T., 2005. The role of viscous heating in Barrovian metamorphism of collisional orogens: thermomechanical models and application to the Lepontine Dome in the Central Alps. J. Metamorph. Geol. 23 (2), 75–95.

Burov, E., Poliakov, A., 2001. Erosion and rheology controls on syn- and post-rift evolution: verifying old and new ideas using a fully coupled numerical model. J. Geophys. Res. 106, 16461–16481.

Burov, E., 2007. The role of gravitational instabilities, density structure and extension rate in the evolution of continental margins. Geol. Soc. (Lond.) Spec. Publ. 282, 139–156.

Burov, E., 2011. Rheology and strength of the lithosphere. Mar. Pet. Geol. 28, 1402–1443.

Burov, E., Gerya, T., 2014. Asymmetric three-dimensional topography over mantle plumes. Nature 513, 85–89. http://dx.doi.org/10.1038/nature13703.

Cloetingh, S., Burov, E., Matenco, L., Beekman, F., Roure, F., Ziegler, P.A., 2013. The Moho in extensional tectonic settings: insights from thermo-mechanical models. Tectonophysics 609, 558–604.

Corti, G., Bonini, M., Conticelli, S., Innocenti, F., Manetti, P., Sokoutis, D., 2003. Analogue modelling of continental extension: a review focused on the relations between the patterns of deformation and the presence of magma. Earth-Sci. Rev. 63, 169–247.

Dunbar, J.A., Sawyer, D.S., 1988. Continental rifting at pre-existing lithospheric weakness. Nature 333, 450–452.

Ellis, G.A., Densmore, A.L., Anderson, R.S., 1999. Development of mountainous topography in the Basin Ranges, USA. Basin Res. 11, 21–41.

Faccenna, C., Becker, T.W., Auer, L., Billi, A., Boschi, L., Brun, J.P., Capitanio, F.A., Funiciello, F., Horvàth, F., Jolivet, L., 2014. Mantle dynamics in the Mediterranean. Rev. Geophys. 52, 283–332. http://dx.doi.org/10.1002/2013RG000444.

Francois, T., Burov, E., Meyer, B., Agard, P., 2013. Surface topography as key constraint on thermo-rheological structure of stable cratons. Tectonophysics 602, 106–123. http://dx.doi.org/10.1016/j.tecto.2012.10.009.

Harangi, S., Jankovics, M.É., Sági, T., Kiss, B., Lukas, R., Soós, I., 2014. Origin and geodynamic relationships of the late Miocene to quaternary alkaline basalt volcanism in the Pannonian basin, eastern-central Europe. Int. J. Earth Sci. 104. http://dx.doi.org/10.1007/s00531–014–1105-7.

Hetényi, Gy., Renc, Y., Dando, B., Stuart, G.W., Hegedűs, E., Kovács, A.Cs., Houseman, G.A., 2015. Crustal structure of the Pannonian Basin: the AlCaPa and Tisza Terrains and the Mid-Hungarian Zone. Tectonophysics 646, 106–116. http://dx.doi.org/10.1016/j.tecto.2015.02.004.

Horváth, F., Musitz, B., Balázs, A., Végh, A., Uhrin, A., Nádor, A., Koroknai, B., Pap, N., Tóth, T., Wórum, G., 2015. Evolution of the Pannonian basin and its geothermal resources. Geothermics 53, 328–352.

Horváth, F., 1995. Phases of compression during the evolution of the Pannonian basin and its bearing on hydrocarbon exploration. Mar. Pet. Geol. 12, 837–844.

Huet, B., Pourhiet, L.L., Labrousse, L., Burov, E., Jolivet, L., 2011. Post-orogenic extension and metamorphic core complexes in a heterogeneous crust, the role of pre-existing nappes. Geophys. J. Int. 184, 611–625. http://dx.doi.org/10.1111/j.1365-246X.2010.04849.x.

Huismans, R.S., Beaumont, C., 2003. Symmetric and asymmetric lithospheric extension: relative effects of frictional-plastic and viscous strain softening. J. Geophys. Res. 108, 2496. http://dx.doi.org/10.1029/2002JB002026.

Huismans, R.S., Podladchikov, Y.Y., Cloetingh, S., 2001. Dynamic modelling of the transition from passive to active rifting, application to the Pannonian basin. Tectonics 20, 1021–1039.

Jolivet, L., Brun, J.P., 2010. Cenozoic geodynamic evolution of the Aegean region. Int. J. Earth Sci. 99, 109–138. http://dx.doi.org/10.1007/s00531-008-0366-4.

Jolivet, L., Faccenna, C., Huet, B., Labrousse, L., Le Pourhiet, L., Lacombe, O., Lecomte, E., Burov, E., Denele, Y., Brun, J.P., Philippon, M., Paul, A., Salaun, G., Karabulut, H., Piromallo, C., Monie, P., Gueydan, F., Okay, A.I., Oberhansli, R., Pourteau, A., Augier, R., Gadenne, L., Driussi, O., 2013. Aegean tectonics: strain localisation, slab tearing and trench retreat. Tectonophysics 597, 1–33.

Kiss, J., 2009. A CEL08 szelvény geofizikai vizsgálata. Mag. Geofiz. 50, 59–74 (Translated: Study of the geophysical data along the CEL08 deep seismic litospheric profile. Hungarian Geophysics).

Kovács, I., Falus, G., Stuart, G., Hidas, K., Szabó, Cs., Flower, M.F.J., Hegedus, E., Posgay, K., Zilahi-Sebess, L., 2012. Seismic anisotropy and deformation patterns in upper mantle xenoliths from the central Carpathian–Pannonian region: asthenospheric flow as a driving force for Cenozoic extension and extrusion? Tectonophysics 514–517, 168–179.

Le Pourhiet, L., Burov, E., Moretti, I., 2004. Rifting through a stack of inhomogeneous thrusts (the dipping pie concept). Tectonics 23, TC4005. http://dx.doi.org/10.1029/2003TC001584.

Lenkey, L., Dovenyi, P., Horvath, F., Cloetingh, S.A.P.L., 2002. Geothermics of the Pannonian Basin and its bearing on neotectonic. In: Cloetingh, S., Horvath, F., Bada, G., Lankreijer, A. (Eds.), Neotectonics and Surface Processes: the Pannonian Basin and Alpine/Carpathians System. In: European Geosciences Union, Stephan Mueller Special Publications, vol. 3, pp. 29–40.

Li, Z.H., Xu, Z.Q., Gerya, T.V., 2011. Flat versus steep subduction: contrasting modes for the formation and exhumation of high- to ultrahigh-pressure rocks in continental collision zones. Earth Planet. Sci. Lett. 301, 65–77.

Liao, J., Gerya, T., 2014. Influence of lithospheric mantle stratification on craton extension: insight from two-dimensional thermo-mechanical modelling. Tectonophysics 631, 50–64.

Matenco, L., Radivojević, D., 2012. On the formation and evolution of the Pannonian Basin: constraints derived from the structure of the junction area between the Carpathians and Dinarides. Tectonics 31, TC6007.

Matenco, L., Munteanu, I., ter Borgh, M., Stanica, A., Tilita, M., Lericolais, G., Dinu, C., Oaie, G., 2016. The interplay between tectonics, sediment dynamics and gateways evolution in the Danube system from the Pannonian Basin to the western Black Sea. Sci. Total Environ. 543, 807–827. http://dx.doi.org/10.1016/j.scitotenv.2015.10.081.

Menant, A., Sternai, P., Jolivet, L., Guillou-Frottier, L., Gerya, T., 2016. 3D numerical modeling of mantle flow, crustal dynamics and magma genesis associated with slab roll-back and tearing: the eastern Mediterranean case. Earth Planet. Sci. Lett. 442, 93–107.

Naliboff, J., Buiter, S.J.H., 2015. Rift reactivation and migration during multiphase extension. Earth Planet. Sci. Lett. 421, 58–67.

Poliakov, A., Cundall, P., Podladchikov, Y., Lyakhovsky, V., 1993. An explicit inertial method for the simulation of viscoelastic flow: an evaluation of elastic effects on diapiric flow in two-and three-layers models. In: Flow and Creep in the Solar System: Observations, Modeling and Theory. Kluwer Academic, Dordrecht, Netherlands, pp. 175–195.

Posgay, K., Bodoky, T., Hajnal, Z., Toth, T.M., Fancsik, T., Hegedus, E., Kovacs, A.C., Takacs, E., 2006. Interpretation of subhorizontal crustal reflections by metamorphic and rheologic effects in the eastern part of the Pannonian Basin. Geophys. J. Int. 167, 187–203.

Ranalli, G., 1995. Rheology of the Earth, second edition. Chapman & Hall, London. 413 pp.

Schmid, S., Bernoulli, D., Fügenschuh, B., Matenco, L., Schefer, S., Schuster, R., Tischler, M., Ustaszewski, K., 2008. The Alpine–Carpathian–Dinaridic orogenic system: correlation and evolution of tectonic units. Swiss J. Geosci. 101, 139–183.

Sokoutis, D., Corti, G., Bonini, M., Brun, J.P., Cloetingh, S., Mauduit, T., Manetti, P., 2007. Modeling the extension of heterogeneous hot lithosphere. Tectonophysics 444, 63–79. http://dx.doi.org/10.1016/j.tecto.2007.08.012.

Tari, G., Dovenyi, P., Dunkl, I., Horvath, F., Lenkey, L., Ştefănescu, M., Szafian, P., Toth, T., 1999. Lithospheric structure of the Pannonian basin derived from seismic, gravity and geothermal data. In: Durand, B., Jolivet, L., Horvath, F., Serrane, M. (Eds.), The Mediterranean Basins: Extension Within the Alpine Orogen. In: Geol. Soc. (Lond.) Spec. Publ., vol. 156, pp. 215–250.

Tesauro, M., Kaban, M.K., Cloetingh, S., 2009. A new thermal and rheological model of the European lithosphere. Tectonophysics 476, 478–495.

Tirel, C., Brun, J.P., Burov, E., 2008. Dynamics and structural development of metamorphic core complexes. J. Geophys. Res. 113, 215–250.

Ustaszewski, K., Kounov, A., Schmid, S.M., Schaltegger, U., Krenn, E., Frank, W., Fügenschuh, B., 2010. Evolution of the Adria–Europe plate boundary in the northern Dinarides: from continent–continent collision to back-arc extension. Tectonics 29, TC6017. http://dx.doi.org/10.1029/2010TC002668.

van Hinsbergen, D.J.J., Schmid, S.M., 2012. Map view restoration of Aegean–West Anatolian accretion and extension since the Eocene. Tectonics 31, TC5005. http://dx.doi.org/10.1029/2012TC003132.

van Wees, J.-D., van Bergen, F., David, P., Nepveu, M., Beekman, F., Cloetingh, S.A.P.L., Bonte, D., 2009. Probabilistic tectonic heat flow modelling for basin maturation: assessment method and applications. Mar. Pet. Geol. 26, 536–551.

Van Wijk, J.W., Cloetingh, S.A.P.L., 2002. Basin migration caused by slow lithospheric extension. Earth Planet. Sci. Lett. 198, 275–288.

Wortel, M.J.R., Spakman, W., 2000. Subduction and slab detachment in the Mediterranean–Carpathian region. Science 209, 1910–1917.

Ziegler, P., Cloetingh, S., 2004. Dynamic processes controlling evolution of rifted basins. Earth-Sci. Rev. 64, 1–50.